Received: 2 January 2017 | Revised: 5 February 2017 | Accepted: 12 February 2017

DOI: 10.1002/aoc.3792

FULL PAPER

WILEY Applied Organometallic Chemistry

Role of Knoevenagel condensate pyrazolone derivative Schiff base ligated transition metal complexes in biological assay and cytotoxic efficacy

Rajakkani Paulpandiyan | Alagarraj Arunadevi | Natarajan Raman

Research Department of Chemistry, VHNSN College, Virudhunagar - 626 001 Tamil Nadu, India

Correspondence
Natarajan Raman, Research Department of Chemistry, VHNSN College, Virudhunagar – 626 001, Tamil Nadu, India.
Email: ramchem1964@gmail.com

A new bioessential Knoevenagel condensate Schiff base ligand (L) was synthesized by the reaction of 3-(4-hydroxy-3-methoxybenzyl)pentane-2,4-dione and 4-aminoantipyrine. The ligand forms monomeric divalent transition metal complexes (**1**–**4**) which were characterized using spectral and analytical data. All these complexes have the general formula $[ML]Cl_2$, where M = Co(II), Ni(II), Cu(II) and Zn(II). They are electrolytic in nature and adopt square planar geometry. The binding propensity of these complexes with calf thymus DNA was investigated using absorption spectrophotometric titration, cyclic voltammetry and viscosity measurements. The binding constant values imply that the complexes bind with DNA via intercalation mode. The *in vitro* antibacterial and antifungal activities reveal that the complexes have good antimicrobial efficacy against a set of pathogens. The nucleolytic cleavage activity of these complexes on pUC18 DNA was investigated using agarose gel electrophoresis. Also, the *in vitro* cytotoxicity of the synthesized complexes against a panel of human tumour cell lines (MCF-7 and HeLa) and normal cell lines (NHDF and HEK) was assayed using the MTT method. Interestingly, complex **1** exhibits more potent anticancer activity than cisplatin and other complexes.

KEYWORDS
human tumour cell lines, intercalation mode, Knoevenagel condensate Schiff base, MTT assay, nucleolytic cleavage

1 | INTRODUCTION

Cancer is reported as a malignant disease causing swift and uncontrolled proliferation of cells. As such, defective cellular apoptosis is essentially involved in the development of cancer.[1] It is major challenge to treat cancer using an appropriate strategy while inducing apoptosis. Anticancer chemotherapy primarily targets damage to DNA and triggers processes such as cell death and prevention of cellular reproduction.[2] Moreover, cell death may be triggered due to apoptosis, since the cell cycle is being constantly prevented.

DNA is identified as a potential biomolecular target during anticancer drug treatment. It is commonly found to bind with metal complexes by covalent as well as non-covalent interactions. A nitrogen base of DNA like guanine N7 can replace the labile covalent binding sites of a ligand employed in a metal complex. Platinum-based anticancer drugs capable of covalently binding to DNA are considered to function efficiently for the extensive treatment of various tumours including testicular, colorectal and lung cancers.[3–5] In particular, the DNA-targeting anticancer chemotherapy drug cisplatin is specifically recommended for the treatment of testicular and ovarian cancers. The results of clinical trials of cisplatin reveal that it is hampered due to the substantial side effects that arise from its binding mode with DNA via an intrastrand crosslink formed between neighbouring guanine residues to a

pair of soft purine nitrogen atoms by covalent binding.[6] In the past two decades, non-platinum metal-based anticancer complexes including those of nickel(II),[7] copper(II),[8] zinc(II)[9] and manganese(II)[10] with potent anticancer activity have been explored in detail. In this respect, much effort has been directed towards the design and synthesis of new metal-based drugs which possess less toxic, more efficacious, target-specific and non-covalent DNA binding.[11]

Moreover, the design of new metal-based drugs must be concerned with enhanced selectivity and distinct modes of DNA interaction like non-covalent interaction which mimic the mode of interaction of proteins with DNA.[12] DNA makes an essential contribution to life processes, since it carries heritage information and induces the biological synthesis of proteins and enzymes by the replication and transcription of genetic information in living cells. DNA is certainly found to be a target substance while using metal complexes, since it provides a variety of options for potential metal binding sites.[13,14] These binding sites employed for the direct covalent coordination to a metal centre are typically electron-rich DNA bases or phosphate groups.

In terms of non-covalent interactions, DNA tends to interact with transition metal complexes by intercalation and groove binding or electrostatic surface binding. In particular, metal complexes containing planar aromatic ligands bind to DNA by intercalation, which is of interest to researchers.[15] Such types of metallointercalators act as strongly mutagenic and exhibit potential chemotherapeutic activity, which is in accord with their DNA binding affinity.[16] In fact any metal complex binding to DNA via an intercalative mode has promising applications. Incidentally, most studies are associated with complexes of ruthenium and selectively with other metal complexes. In order to develop an original metal complex with new structure–pharmacological activity relationship, it is very critical to understand its DNA binding properties and its prospective interaction leading to cytotoxicity in tumour cells.

Currently, chemotherapeutic Knoevenagel condensate Schiff bases are the focus of biochemists. Condensation of the active methylene group of a β-diketone with an aldehyde substrate affords a non-enolizable Knoevenagel condensate which can effectively react with amines to form quantitatively a Schiff base ligand which possesses favourable coordination sites for the formation of stable transition metal complexes.[17] Pyrazol-3-one can generate a set of promising compounds with extensive pharmacological properties including analgesic, antipyretic and antirheumatic activities.[18] Indeed, a Schiff base ligand of pyrazol-3-one is liable to exhibit enhanced biological activities as a requisite as a pharmacophore in various pharmacologically active agents.[19] In addition, the Knoevenagel condensate Schiff base metal complexes developed in recent times have been explored widely in various applications like agriculture, industry, pharmaceutical, etc.[20,21]

Based on the above considerations, we have synthesized a Schiff base ligand (L) derived from the condensation reaction of 3-(4-hydroxy-3-methoxybenzyl)pentane-2,4-dione with 4-aminoantipyrine as well as its respective Co(II), Ni(II), Cu(II) and Zn(II) complexes of the structure type $[ML]Cl_2$ (where L is a tetradentate Knoevenagel condensate ligand). Their scope and merits were studied on the basis of characterizations like UV absorption titration, viscosity measurements, cyclic voltammetry and electrophoresis technique to probe the DNA interaction of these metal complexes. Further, all the synthesized compounds were screened for their *in vitro* antimicrobial activity against various bacterial and fungal strains. The cytotoxicity of the synthesized compounds was investigated against human cancer cell lines such as breast adenocarcinoma (MCF-7) and cervical carcinoma (HeLa) cell lines and non-cancerous human normal cell lines such as dermal fibroblast (NHDF) and embryonic kidney (HEK) cell lines using MTT assay.

2 | EXPERIMENTAL

The materials and methods involved in the DNA binding interaction and DNA cleavage efficacy investigations, antimicrobial screening and cell proliferation assay are given in the supporting information (S1).

2.1 | Synthesis of Knoevenagel condensate β-Diketone ligand

The non-enolizable β-diketone 3-(4-hydroxy-3-methoxybenzyl)pentane-2,4-dione was prepared using the following procedure. Acetylacetone (1.0 g, 10 mmol) and 4-hydroxy-3-methoxybenzaldehyde (1.52 g, 10 mmol) were dissolved in ethanol (40 ml) in the presence of piperidine (0.05 ml). The reaction mixture was stirred homogeneously for *ca* 5 h with occasional cooling and incubated in a refrigerator for two days. The yellow-coloured crystalline solid obtained from the cold reaction mixture was filtered and washed with ethanol followed by an excess of petroleum ether to eliminate the unreacted precursors. Washing was repeated three times and the compound was recrystallized from ethanol. This compound was used as one component for the synthesis of the new Schiff base (L).

Yield 78%; yellow colour. Anal. Calcd for $C_{13}H_{16}O_4$ (%): C, 66.1; H, 6.8. Found (%): C, 65.6; H, 6.1. FT-IR (KBr, cm^{-1}): 1710 (C═O), 3420 (─OH). ^{1}H NMR (DMSO-d_6, δ, ppm): 6.8–7.2 (m, Ar-H, 3H), 2.2 (s, C─CH_3, 6H), 2.6 (s, ─CH_2, 2H), 3.2 (s, ─CH, 1H), 3.8 (s, OCH_3, 3H), 9.6 (s, OH, 1H). UV–visible (DMSO, cm^{-1} (transition)): 35 122 (π–π*).

2.2 | Synthesis of Schiff Base (L)

The dissolution of 3-(4-hydroxy-3-methoxybenzyl)pentane-2,4-dione (1.1 g, 5 mmol), prepared as described above, with 4-aminoantipyrine (2.0 g, 10 mmol) was carried out in ethanol (40 ml) and refluxed for *ca* 4 h with vigorous stirring and allowed to attain room temperature. Then the reaction mixture was poured into crushed ice to afford orange crystals, which were filtered and recrystallized from ethanol and dried under vacuum. The route for the synthesis and the proposed molecular structure of L with respect to spectral data are shown in Scheme 1.

Yield 72%; orange colour. Anal. Calcd for $C_{35}H_{36}N_6O_4$ (%): C, 69.5; H, 6.0; N, 13.9. Found (%): C, 68.3; H, 5.8; N, 13.6. FT-IR (KBr, cm^{-1}): 1654 (C═O), 1590 (C═N), 3425 (─OH). ^{1}H NMR (DMSO-d_6, δ, ppm): 7.1–7.5 (m, Ar-H, 13H), 3.4 (s, C═C─CH_3, 6H), 2.4 (s, N═C─CH_3, 6H), 3.1 (s, N─CH_3, 6H), 6.8 (s, HC═C, 1H), 3.8 (s, OCH_3, 3H), 9.5 (s, OH, 1H). ^{13}C NMR (DMSO-d_6, δ, ppm): 118.9 (C_1 and C_4), 146.9 (C_2), 148.1 (C_3), 108.5 (C_5), 114.4 (C_6), 55.9 (C_7), 123.2 (C_8), 124.3 (C_9), 157.4 (C_{10}), 18.01 (C_{11}), 144.1 (C_{12}), 151.3 (C_{13}), 163.0 (C_{14}), 10.18 (C_{15}), 35.96 (C_{16}), 134.8 (C_{17}), 126.8 (C_{18} and C_{22}), 130.6 (C_{19} and C_{21}), 129.1 (C_{20}). UV–visible (DMSO, cm^{-1} (transition)): 35 842 (π–π*), 29 412 (n–π*).

2.3 | Synthesis of metal complexes (1–4)

A solution of M(II) chloride (M = Cu, Co, Ni and Zn) in ethanol (1 mmol) was mixed with an ethanolic solution of Schiff base L (1 mmol) and the resultant mixture was refluxed for *ca* 3 h. The progress of the reaction was continuously monitored with the aid of TLC. The solid complex precipitated from the solution was filtered off and washed thoroughly with ethanol followed by petroleum ether and dried over anhydrous $CaCl_2$ under vacuum.

[CuL]Cl_2 (1). Yield 62%; brown colour. Anal. Calcd for $CuC_{35}H_{36}N_6O_4Cl_2$ (%): C, 56.9; H, 4.9; N, 11.4; Cu, 8.6. Found (%): C, 56.2; H, 4.8; N, 11.1; Cu, 8.5. FT-IR (KBr, cm^{-1}): 1575 (─C═N), 1624 (─C═O), 3420 (─OH), 505 (M─O), 445 (M─N). Λ_m (Ω^{-1} mol^{-1} cm^2): 148. μ_{eff} (BM): 1.82. UV–visible (DMSO, cm^{-1} (transition)): 16 181 (d–d).

[CoL]Cl_2 (2). Yield 60%; pale green colour. Anal. Calcd for $CoC_{35}H_{36}N_6O_4Cl_2$ (%): C, 57.2; H, 4.9; N, 11.4; Co, 8.0. Found (%): C, 56.8; H, 4.8; N, 11.0; Co, 7.9. FT-IR (KBr, cm^{-1}): 1580 (─C═N), 1630 (─C═O), 3410 (─OH), 515 (M─O), 460 (M─N). Λ_m (Ω^{-1} mol^{-1} cm^2): 125. μ_{eff} (BM): 3.24. UV–visible (DMSO, cm^{-1} (transition)): 16 313 (d–d).

[NiL]Cl_2 (3). Yield 68%; brownish yellow colour. Anal. Calcd for $NiC_{35}H_{36}N_6O_4Cl_2$ (%): C, 57.3; H, 4.9; N, 11.4; Ni, 8.0. Found (%): C, 57.0; H, 4.8; N, 11.1; Ni, 7.7. FT-IR (KBr, cm^{-1}): 1572 (─C═N), 1636 (─C═O), 3400 (─OH), 520 (M─O), 452 (M─N). Λ_m (Ω^{-1} mol^{-1} cm^2): 139. UV–visible (DMSO, cm^{-1} (transition)): 16 393 (d–d).

[ZnL]Cl_2 (4). Yield 66%; pale yellow colour. Anal. Calcd for $ZnC_{35}H_{36}N_6O_4Cl_2$ (%): C, 56.7; H, 4.9; N, 11.3; Zn, 8.8. Found (%): C, 56.2; H, 4.7; N, 11.2; Zn, 8.7. FT-IR (KBr, cm^{-1}): 1570 (─C═N), 1635 (─C═O), 3422 (─OH), 512 (M─O), 465 (M─N). ^{1}H NMR (DMSO-d_6, δ, ppm): 7.1–7.5 (m, Ar-H, 13H), 3.4 (s, C═C─CH_3, 6H), 2.4 (s, N═C─CH_3, 6H), 3.1 (s, N─CH_3, 6H), 6.8 (s, HC═C, 1H), 3.8 (s, OCH_3, 3H), 9.5 (s, OH, 1H). ^{13}C NMR (DMSO-d_6, δ, ppm): 117.4 (C_1 and C_4), 146.4 (C_2), 148.6 (C_3), 108.0 (C_5), 114.9 (C_6), 56.9 (C_7), 122.5 (C_8), 124.7 (C_9), 155.4 (C_{10}), 18.32 (C_{11}), 144.1 (C_{12}), 151.1 (C_{13}), 163.4 (C_{14}), 10.33 (C_{15}), 36.12 (C_{16}), 135.2 (C_{17}), 127.1 (C_{18} and C_{22}), 130.7 (C_{19} and C_{21}), 129.5 (C_{20}). Λ_m (Ω^{-1} mol^{-1} cm^2): 128. μ_{eff} (BM): diamagnetic. UV–visible (DMSO, cm^{-1} (transition)): 32 256 (ligand–metal charge transfer).

3 | RESULTS AND DISCUSSION

All the metal(II) complexes (**1**–**4**) were obtained upon reaction between metal ion and ligand at a metal-to-ligand molar

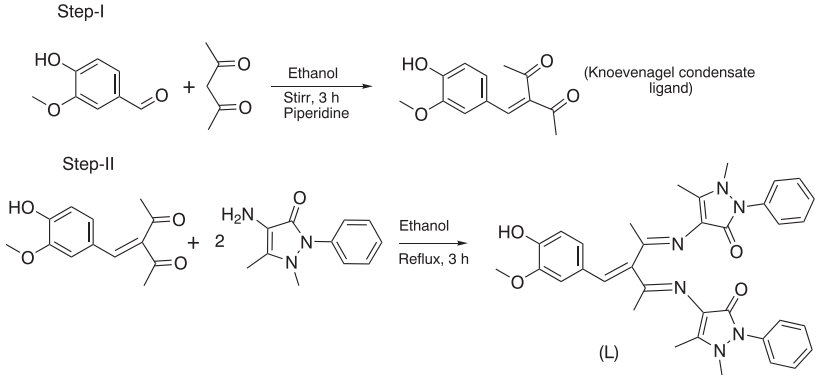

SCHEME 1 Route for the synthesis of Knoevenagel condensate Schiff base (L)

ratio of 1:1. These synthesized complexes exist as stable compounds at room temperature which are soluble in DMF and DMSO, while insoluble in water and many common organic solvents. Analytical data of these complexes support the proposed general formula $[ML]Cl_2$. The experimental elemental analyses data of the compounds are found to be in good agreement with the calculated data. The magnetic susceptibility data imply the monomeric nature of these complexes. In addition, the high conductance values of these metal complexes indicate their electrolytic properties due to the existence of counter ions in the proposed structure of complexes **1**–**4**. The proposed molecular structure of the Knoevenagel condensate Schiff base complexes is depicted in Figure 1.

3.1 | Fourier transform infrared (FT-IR) spectra

FT-IR spectra of ligand L and its respective metal complexes **1**–**4**, recorded in the region 400–4000 cm^{-1}, are shown in Figure S1. The spectra of the complexes are compared with that of the free ligand in order to identify the coordination sites which contribute to chelation. The azomethine nitrogen (─C═N) stretching frequency appears at 1590 cm^{-1} for the free ligand whereas for the metal complexes the signal shifts towards lower wavenumber around 1562–1580 cm^{-1}. The shift in frequency occurs due to the coordination of imine groups towards the metal centre.[22] Similarly the band corresponding to the carbonyl oxygen (─C═O) stretching frequency at 1654 cm^{-1} (L) is shifted to 1624–1638 cm^{-1} due to the coordination of carbonyl oxygen atom of the ligand to the metal centre. A strong broad band is noticed in the range 3400–3425 cm^{-1} for both the free ligand and its complexes, which is due to the phenolic ─OH group of vanillin moiety that implies the unbounded nature in coordination.[23] The spectrum of each metal complex exhibits slightly less intense bands in the regions 445–460 and 505–520 cm^{-1} which indicate the formation of (M─N) and (M─O) bonds, respectively.[24]

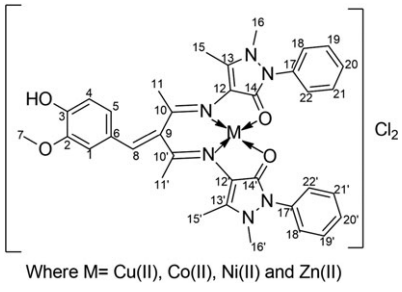

FIGURE 1 Proposed structure of the Knoevenagel condensate Schiff base complexes

3.2 | Electronic absorption spectra and magnetic moments

The absorption spectra and magnetic data can afford ready and reliable information about the ligand arrangement around the metal centre in transition metal complexes. This is employed as an essential tool to distinguish between the geometries of complexes. Electronic spectra of L and its complexes were recorded in the range 200–1100 nm at room temperature in DMSO medium. The absorption spectra of L and its metal complexes are shown in Figure S2. The absorption spectrum of L exhibits two characteristic bands at 35 842 and 29 412 cm^{-1} which correspond to the intraligand charge transfer transitions of $\pi \rightarrow \pi^*$ and $n \rightarrow \pi^*$, respectively. These two transitions are shifted due to complex formation, either a bathochromic or hypsochromic shift.

In the case of complex **1**, a strong absorption d–d band appears at 16 181 cm^{-1}, assigned to $^2B_{1g} \rightarrow {}^2A_{1g}$ transition, which is characteristic of square planar geometry.[25] This is further supported by the magnetic susceptibility value (1.82 BM). Moreover, a d–d band at 16 393 cm^{-1} for complex **2** represents the $^1A_{1g} \rightarrow {}^1B_{1g}$ transition, which also implies square planar geometry. In fact the magnetic moment value (3.24 BM) of this d^7 Co(II) ion complex supports the square planar stereochemistry around the metal centre.[26] Similarly, the d–d band at 16 393 cm^{-1} for complex **3** can also be assigned to $^1A_{1g} \rightarrow {}^1B_{1g}$ transition and square planar geometry is identified from the observed diamagnetic value of this complex. Obviously, complex **4** does not show any band in the visible region due to the diamagnetic behaviour of the Zn(II) ion in the complex.

3.3 | ^{1}H NMR and ^{13}C NMR spectra

In the case of ^{1}H NMR spectra, the peak assignment for the proton resonances was based on their peak multiplicity, intensity pattern and correlation of the integration values of the protons with the predicted pattern. The ^{1}H NMR spectra of L and its diamagnetic Zn(II) complex **4** (Figures S3 and S4) were recorded in DMSO-d_6 using tetramethylsilane as the internal standard. The ^{1}H NMR spectrum of L shows peaks at 7.1–7.5 ppm (m, 13H) and 9.5 ppm (s, 1H) attributed to the phenyl multiplet and the phenolic ─OH group of the 4-hydroxy-3-methoxybenzaldehyde moiety of L. It also shows the following signals: C═C─CH_3 at 3.4 ppm (s, 6H), N═C─CH_3 at 2.4 ppm (s, 6H), N─CH_3 at 3.1 ppm (s, 6H), HC═C at 6.8 ppm (s, 1H) and OCH_3 at 3.8 ppm (s, 3H). The signal for the phenolic ─OH proton is observed in the spectrum of Zn(II) complex **4** which reveals that ─OH proton exists free from sequestration. Likewise there is no significant alteration perceived with the remaining signals of this spectrum.

The ^{13}C NMR spectra of L and its complex **4** are depicted in Figures S5 and S6. The signals of aromatic carbons of L are identified in the range 119–148 ppm. Moreover, the imine group (C═N) and carbonyl (C═O) carbons are observed at 157 and 163 ppm. In the spectrum of complex **4**, it is observed that these peaks are shifted to downfield region, specifying the coordination of (C═N) and (C═O) groups towards the metal centre. There is no such marked difference noted with other signals in this spectrum.

3.4 | Electron paramagnetic resonance (EPR) spectra

The X band EPR spectrum of complex **1** was recorded in DMSO medium at room temperature and liquid nitrogen temperature at a frequency of 9.1 GHz under a magnetic field strength of 3000 G (Figure S7). The spin Hamiltonian parameters of complex **1** were calculated and are summarized in Table 1. Based on the spectral data, it is noted that $A_{\parallel}$ (131) > $A_{\perp}$ (26); $g_{\parallel}$ (2.18) > $g_{\perp}$ (2.04) > 2.0027, which reveal that the unpaired electron is most likely to localize in $d_{x^2-y^2}$ orbital of Cu(II) ion, scaffolding the square planar geometry.[27] In accordance with g factors, the geometric parameter G is determined, indicating a measure of exchange interaction between Cu(II) centres in polycrystalline compound:

$$G = \frac{g_{\parallel} - 2.0027}{g_{\perp} - 2.0027} \quad (1)$$

This measures the exchange interaction between the copper centres in polycrystalline solid. The resultant value ($G = 4.5$) for the exchange interaction parameter for complex **1** verifies a negligible exchange interaction among Cu–Cu in complex **1** according to Hathaway and Tomlinson.[28]

The degree of geometrical distortion ($g_{\parallel}/A_{\parallel}$) is observed as an index of deviation from idealized geometry; a value below 120 cm^{-1} is typically known for planar complexes, whereas the range 120 to 180 cm^{-1} is characteristic of minor to moderate distortion and 180–250 cm^{-1} indicates a major distortion towards tetrahedron.[29] The $g_{\parallel}/A_{\parallel}$ value obtained (166 cm^{-1}) for the synthesized complex **1** is in good agreement with appreciable deviation from planarity which is further supported by the bonding parameter (α^2) value which is less than unity. The covalency parameters α^2 (covalent in-plane σ-bonding) and β^2 (covalent in-plane π-bonding) were calculated from the following equations:

$$\alpha^2 = \frac{A_{\parallel}}{0.036} + (g_{\parallel} - 2.0027) + \frac{3}{7}(g_{\perp} - 2.0027) + 0.04 \quad (2)$$

$$\beta^2 = (g_{\parallel} - 2.0027)\left(\frac{E}{-8\lambda\alpha^2}\right) \quad (3)$$

where $\lambda = -828$ cm^{-1} for the free copper ion and E is the electronic transition energy. In the case of complexes, $\alpha^2 = 0.5$ specifies absolute covalent bonding, whereas $\alpha^2 = 1.0$ implies pure ionic bonding. In the present case, the calculated values of α^2 (0.74) and β^2 (0.96) indicate that the in-plane σ-bonding and in-plane π-bonding are appreciably covalent and are consistent with strong in-plane π-bonding in this complex. Based on the above parameters, complex **1** is presumed to exist in square planar geometry. Thus, the EPR data for complex **1** provide evidence to corroborate the conclusion drawn on the basis of electronic spectrum and magnetic moment value as well.

TABLE 1 Spin Hamiltonian parameters of complex **1** in DMSO solution at liquid nitrogen temperature

	g-tensor			*A* (× 10^{-4} cm^{-1})				
Complex 1	$g_{\parallel}$	$g_{\perp}$	g_{iso}	$A_{\parallel}$	$A_{\perp}$	A_{iso}	$g_{\parallel}/A_{\parallel}$	G
$[CuL]Cl_2$	2.18	2.04	2.09	131	26	61	166	4.5

3.5 | Mass spectra

Electron spray ionization mass data of the free ligand and its complexes were obtained to determine their molecular weight and study their fragmentation patterns. The mass spectra of L and its complex **1** are displayed in Figure S8. The mass spectrum of L shows the molecular ion peak at m/z 604 with respect to $[C_{35}H_{36}N_6O_2]^+$ ion. Also the spectrum exhibits peaks for fragments at m/z 481, 228, 188, 123 and 107, indicating the possible fragmented species $[C_{28}H_{29}ON_6O_2]^+$, $[C_{13}H_{14}N_3O]^+$, $[C_{11}H_{12}N_2O]^+$, $[C_7H_7O_2]^+$ and $[C_7H_7O]^+$. The mass spectrum of $[CuL]^+$ complex shows molecular ion peak at m/z 669 [M + 1] which is equivalent to its molecular weight. Complex **1** exhibits additional fragment ion peaks at m/z 604, 481, 228, 188, 123 and 107 corresponding to $[C_{35}H_{36}N_6O_2]^+$, $[C_{28}H_{29}ON_6O_2]^+$, $[C_{13}H_{14}N_3O]^+$, $[C_{11}H_{12}N_2O]^+$, $[C_7H_7O_2]^+$ and $[C_7H_7O]^+$. Based on the observed m/z values or fragmentation patterns of L and its complex, the stoichiometry of the complex is $[ML]Cl_2$.

3.6 | DNA binding studies

3.6.1 | Absorption spectral titrations

UV–visible absorption spectroscopy is commonly used to analyse the binding mode of metal complexes with DNA.[30] DNA can bind to metal complexes via covalent and/or non-covalent interactions. In the case of covalent binding, a labile ligand of a complex can be substituted by nitrogen base of DNA such as guanine (N7), whereas the non-covalent interactions include intercalative, electrostatic and groove (surface) binding of metal complexes outside of

the DNA helix, along major/minor groove.[31] The interaction between a complex and DNA is assumed to perturb the ligand-centred transitions of the complex. In this context, absorption spectra of the complexes were obtained in the presence or absence of calf thymus DNA (CT DNA) at various concentrations. Hyperchromism and hypochromism are two different spectral features of DNA concomitant to its double helix structure, wherein hyperchromism arises from the alternation of the secondary structure of DNA and hypochromism arises from the contraction of DNA in its helix axis as well as from the conformational variation of DNA.[32] During intercalation, π* orbital of the intercalated ligand can couple with the π orbital of DNA base pairs which leads to bathochromism due to the reduction of π → π* transition energy. On the other hand, the coupling of π orbital favours partial electron filling, thus inhibiting the transition probabilities and concomitantly showing hypochromism.[33]

The absorption spectra of complex **1** in the absence and presence of CT DNA in the UV region are shown in Figure 2. The absorption parameters of complexes **1**–**4** bound to CT DNA are listed in Table 2. A marginal hypochromic shift in the intraligand transition is identified with all four complexes upon addition of CT DNA in increasing quantity with a red shift (2–4 nm). This implies that these complexes interact with CT DNA through the intercalative mode with a strong interaction between the complexes and the base pairs of DNA.[34] The planarity and extended aromaticity of the Knoevenagel condensate Schiff base ligand unit promote the stacking of the molecule among the DNA bases. This study shows the trend of hypochromism among the synthesized complexes follows the order **1** > **4** > **3** > **2**, with the binding constant (K_b) varying between 2.6×10^5 and 4.5×10^5 M^{-1} (Table 2). Binding constant values of these complexes indicate that complex **1** has the maximum binding affinity since

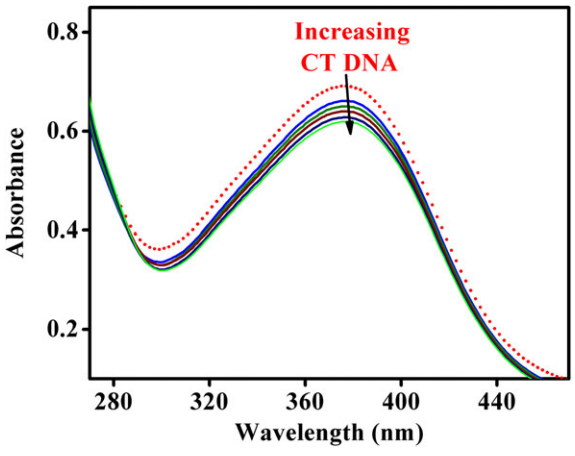

FIGURE 2 Absorption spectra of complex **1** in the absence (dashed curve) and presence (solid curves) of CT DNA in 5 mM Tris–HCl/50 mM NaCl (pH = 7.2) at 25 °C. Arrow indicates the change in absorbance with increasing DNA concentration

TABLE 2 Electronic absorption parameters for interaction of CT DNA with complexes

Complex	λ_{max} (nm) Free	λ_{max} (nm) Bound	$\Delta\lambda$ (nm)	H (%)[a]	K_b ($\times 10^5$ M^{-1})[b]
1	376	376.8	0.8	9.6	4.5
2	378	379.6	1.6	4.4	2.6
3	382	384.0	2.0	4.9	3.2
4	380	381.0	1.0	5.6	3.8

[a]$H = [(A_{free} - A_{bound})/A_{free}] \times 100\%$.

[b]Error limit: ±2%.

it possesses large hydrophobic contacts and π–π stacking of the DNA bases, while the other complexes act as moderate binders. In particular, the observed binding constant values are found to be much higher than that of the effective anticancer drug cisplatin ($3.20 \pm 0.15 \times 10^4$ M^{-1})[35] and less than that of ethidium bromide (1.4×10^6 M^{-1}).[36]

3.6.2 | Electrochemical behaviour

The electrochemical method is an important tool in examining the type and approach of DNA binding with metal complexes. Cyclic voltammetry was chosen to understand the electrochemical properties of the complexes. Cyclic voltammetric studies of the complexes were conducted in DMSO (10^{-3} M) at a sweep rate of 0.5 V s^{-1} in the potential range + 2 to −2 V. The characteristic cyclic voltammograms of complex **1** are depicted in Figure 3 and quasi-reversible redox couple for each complex has been analysed upon the addition of CT DNA and shifts of $E_{1/2}$ and ΔE_p are presented in Table 3.

The incremental addition of CT DNA leads to a substantial drop in the voltammetric current of the redox wave with a slight shift in $E_{1/2}$ to positive potential. The drop in current

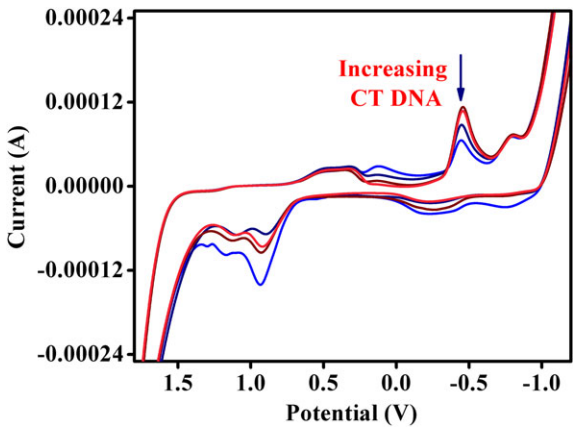

FIGURE 3 Cyclic voltammograms of complex **1** in 5 mM Tris–HCl/50 mM NaCl (pH = 7.2) at 25 °C in presence of increasing amounts of CT DNA

TABLE 3 Electrochemical parameters for interaction of CT DNA with complexes

	$E_{1/2}$ (V)[a]		ΔE_p (V)[b]		
Complex	**Free**	**Bound**	**Free**	**Bound**	I_{pa}/I_{pc}
1	0.248	0.356	1.325	1.426	0.91
2	−0.287	−0.161	1.566	1.784	0.89
3	−0.512	0.623	1.002	2.106	0.84
4	0.567	0.778	1.497	1.506	0.66

[a]$E_{1/2} = (E_{pa} + E_{pc})/2$.

[b]$\Delta E_p = E_{pa} - E_{pc}$.

intensity can be elucidated in terms of an equilibrium mixture of free and DNA-bound complexes at the electrode surface.[37] This condition reveals that the complex stabilizes the duplex (GC pairs) by an intercalating mode. Evidently, the decline of the voltammetric currents in the presence of DNA may be accounted for by the hindered diffusion of the metal complex bound to CT DNA. Both cathodic and anodic peaks show positive or negative shift which specifies the intercalation of complex to DNA base pairs.[38]

3.6.3 | Viscosity measurements

To further investigate the binding nature of the complexes with DNA, viscosity was measured after the incubation of DNA solutions with the complexes. Hydrodynamic measurement which differs with respect to length variation (i.e. viscosity and sedimentation) is considered as the least ambiguous as well as the essential test for the binding model in solution, when crystallographic data are unavailable.[39] To explore the binding mode of complexes with CT DNA, change in viscosity of DNA at room temperature was measured on varying the complex concentration. A typical intercalative mode causes a major enhancement in viscosity of DNA solution due to the appreciable separation of base pairs at intercalation sites, leading to an overall increase in DNA length. In contrast, complexes which bind absolutely in the DNA grooves by partial and/or non-classical intercalation, under identical conditions, generally cause less of a change (positive or negative) or no change in viscosity of DNA solution.[40] The effects of all the synthesized complexes on the viscosity of DNA at 30 ± 0.1 °C are shown in Figure 4. Viscosity measurement results evidently show that each complex can intercalate between adjacent DNA base pairs, initiating an extension in the helix and increasing the viscosity of DNA. When the concentration of the complex is increased, the complexes can intercalate strongly, leading to a larger increase in viscosity of DNA. Therefore, based on spectroscopic studies along with viscosity measurements, it can be perceived that these complexes bind with the DNA via intercalation mode.

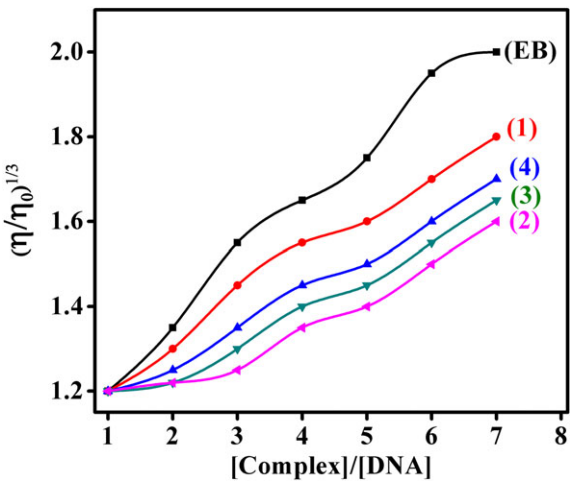

FIGURE 4 Effect of increasing amounts of ethidium bromide (EB) and complexes **1**–**4** on the relative viscosity of CT DNA. Plot of relative viscosity $(\eta/\eta_0)^{1/3}$ versus [complex]/[DNA]

3.6.4 | Agarose gel electrophoresis

The agarose gel pattern of plasmid DNA is accounted for by two distinct conformations, one is supercoiled DNA (Form I) and the other is nicked circular DNA (Form II). Altogether, the relaxed form of plasmid DNA is formed due to the cleavage of the DNA strands (nicking of DNA), known as the nicked circular form, which migrates very slowly in agarose gel. The linear form of DNA (Form III) is generated to migrate between supercoiled and nicked circular forms, if both strands are cleaved.[41] Agarose gel electrophoresis can differentiate all three different plasmid DNA conformations during analysis.

3.6.5 | Absence of activators

We deduce that complex **1** shows binding tendency with CT DNA exclusively. The cleavage activity is examined using supercoiled pUC18 DNA. It is incubated with different concentrations (control, 20, 40, 60, 80 and 100 μM) of complex **1** in Tris–borate–EDTA buffer at pH = 7.2 for 3 h, free from any activating agents. With increasing concentration of **1**, the ratio of Form I reduces gradually and there is partial transformation to Form II with concurrent increase in the intensity of the latter form, whereas the production of Form III also increases at 100 μM (Figure 5, lane 6). Thus, in the absence of activators, the concentration-dependent cleavage of pUC18 DNA is observed in the case of complex **1** as shown in Figure 5.

3.6.6 | Presence of activators

Moreover, DNA cleavage was evaluated by detecting the transformation of supercoiled to linear form in the presence

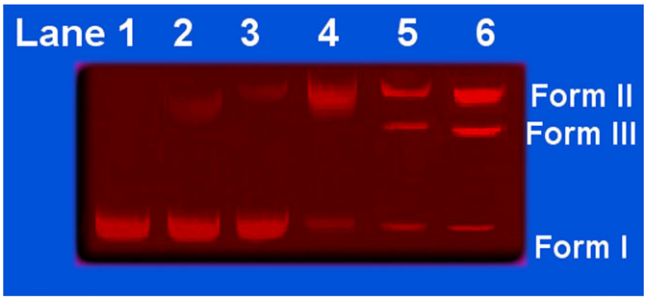

FIGURE 5 Gel electrophoresis pattern showing cleavage of pUC18 DNA (30 μM) by complex **1** at 35 °C after 2 h of incubation. Lane 1: DNA control; lane 2: 20 μM of **1** + DNA; lane 3: 40 μM of **1** + DNA; lane 4: 60 μM of **1** + DNA; lane 5: 80 μM of **1** + DNA; lane 6: 100 μM of **1** + DNA

of activators. Figure 6 represents the cleavage of pUC18 DNA stimulated by the metal complexes in the presence of H_2O_2 as oxidant. Control experiments with DNA itself failed to indicate any considerable cleavage of pUC18 DNA, even upon long exposure period (lane 1). The ratio of supercoiled form (Form I) reduced constantly and partly transformed to nicked form (Form II), and the intensity of the Form II band increased and transformed to Form III by the complexes even at a concentration of 20 μM. Each complex tends to exhibit a pronounced cleavage activity in the presence of H_2O_2. This may be responsible for the formation of hydroxyl free radicals. It is manifested that complex **1** possesses high ability to cleave the supercoiled plasmid DNA as compared to the other complexes. These observations imply that DNA alters its conformation due to the binding of the metal complexes. The generation of a hydroxyl radical upon reaction of metal complex with oxidant may be described as follows:

$$M(II) + e^- \rightarrow M(I)$$
$$M(I) + O_2 \rightarrow M(II) + O_2^-$$
$$2O_2^- + 2H^+ \rightarrow H_2O_2 + O_2$$
$$M(I) + H_2O_2 \rightarrow M(II) + OH^- + OH^\bullet$$
$$O_2^- + H_2O_2 \rightarrow O_2 + OH^- + OH^\bullet$$

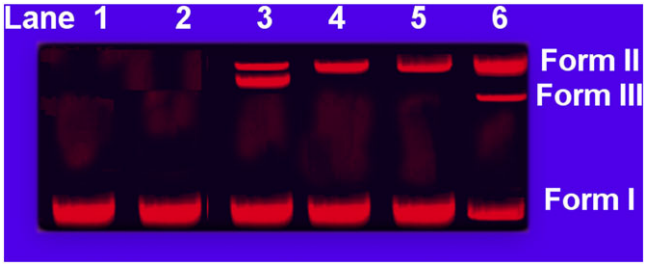

FIGURE 6 Gel electrophoresis pattern showing cleavage of pUC18 DNA (30 μM) treated with L and its metal complexes **1**–**4** (20 μM) at 35 °C after 2 h of incubation. Lane 1: DNA control; lane 2: DNA + L+ H_2O_2; lane 3: DNA + **1** + H_2O_2; lane 4: DNA + **2** + H_2O_2; lane 5: DNA + **3** + H_2O_2; lane 6: DNA + **4** + H_2O_2

The above OH free radicals are employed to oxidize the deoxyribose moiety as well as the hydrolytic cleavage of sugar phosphate backbone.[42,43] Further studies in this direction would assist to envisage the exact mechanistic pathway in cleavage reactions involved in radical scavengers and reactive oxygen species of metal complexes with plasmid DNA.

3.7 | Antimicrobial activity

The antimicrobial activity of the synthesized compounds towards biological systems is an intriguing aspect in current research. The *in vitro* antimicrobial activity of the synthesized free ligand and its metal complexes was tested against various microorganisms, namely two Gram-positive bacteria (*Staphylococcus aureus* and *Bacillus subtilis*), three Gram-negative bacteria (*Escherichia coli*, *Klebsiella pneumoniae* and *Salmonella typhi*) and five fungi (*Aspergillus niger*, *Fusarium solani*, *Curvularia lunata*, *Rhizoctonia bataticola* and *Candida albicans*), using the broth dilution method. Fluconazole and kanamycin were chosen as standards for fungi and bacteria, respectively. The minimum inhibitory concentration (MIC) values against the strains of bacteria and fungi are shown in Figures 7 and 8, respectively.

Tables 4 and 5 summarize the MIC values of the complexes under investigation. The data for the antibacterial and antifungal activity reveal that the metal chelates exhibit potential activity as compared to free ligand against the same microorganisms due to the greater lipophilic nature of the complexes, under identical experimental conditions.[44] This tends to suggest that the chelation could facilitate the ability of a complex to cross a cell membrane according to Tweedy's chelation theory.[45] Chelation significantly reduces the polarity of the metal ion due to the partial sharing of its positive charge with donor groups and possible electron delocalization over the whole chelate ring. Such type of chelation could improve the lipophilic properties of the

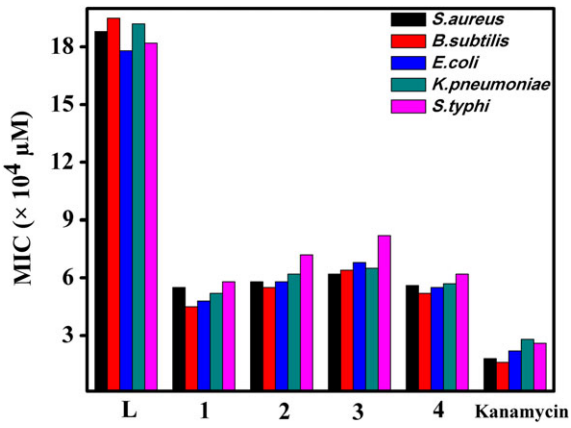

FIGURE 7 Antibacterial activity of synthesized compounds against various pathogens

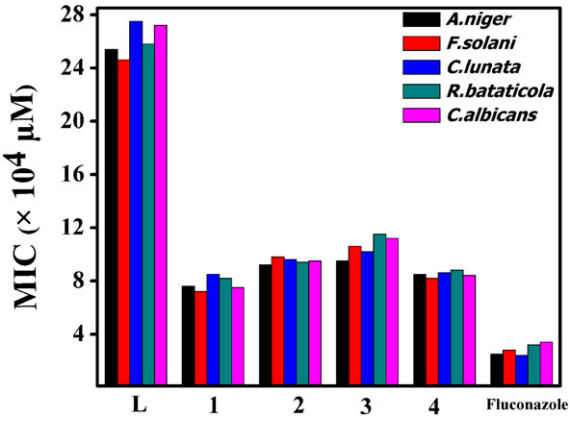

FIGURE 8 Antifungal activity of synthesized compounds against various pathogens

TABLE 4 Minimum inhibitory concentration (MIC) of synthesized compounds against growth of bacteria

	MIC (× 10^4 μM); SEM = ±1.5				
Compound	***S. aureus***	***B. subtilis***	***E. coli***	***K. pneumoniae***	***S. typhi***
L	15.8	16.5	16.2	17.2	15.2
1	3.2	3.5	3.8	4.2	4.0
2	5.2	5.8	5.6	5.2	5.4
3	6.5	6.2	6.8	2.2	6.4
4	4.5	4.2	4.5	4.7	4.2
Kanamycin[a]	1.8	1.6	2.2	2.8	2.6

[a]Kanamycin used as standard.

TABLE 5 Minimum inhibitory concentration (MIC) of synthesized compounds against growth of fungi

	MIC (× 10^4 μM); SEM = ±2				
Compound	***A. niger***	***F. solani***	***C. lunata***	***R. bataticola***	***C. albicans***
L	25.4	24.6	27.5	25.8	27.2
1	7.6	7.2	8.5	8.2	7.5
2	9.2	9.8	9.6	9.4	9.5
3	9.5	10.6	10.2	11.5	11.2
4	8.5	8.2	8.6	8.8	8.4
Fluconazole[a]	2.5	2.8	2.4	3.2	3.4

[a]Fluconazole used as standard.

central metal atom, which consequently favours its permeation through the lipid layer of the cell membrane. In particular, complex **1** shows a higher antifungal activity and antibacterial activity than the other complexes. This higher activity of the copper complex is deduced from the fact that increasing the size of the metal ion decreases the polarization which is further explained on the basis of chelation theory.[45] The variation in the efficiency of the various complexes against diverse organisms depends on the impermeability of the cells of the microbes or on the variation in ribosome of the microbial cells.[46]

3.8 | *In Vitro* cytotoxicity

The promising results observed from the earlier studies concerned with this work revealing the potential to act as cancer chemotherapeutic agents prompted us to evaluate the *in vitro* cytotoxic activity of the synthesized compounds. The *in vitro* anticancer activity was evaluated against a couple of cancer cell lines, MCF-7 and HeLa, and a couple of non-cancerous cell lines, NHDF and HEK, using MTT assay with cisplatin as standard (positive control). The cell lines were treated with the synthesized compounds at a range of concentrations (0–100 μM) for 48 h. The results were analysed by means of cell inhibition expressed as IC_{50} values, which are listed in Table 6.

Complexes **1**–**4** show higher cytotoxic activity against cell lines HeLa and MCF-7. Among the complexes studied, complex **1** has significantly stronger inhibitor effect on the proliferation of HeLa and MCF-7 cells than cisplatin under similar experimental conditions. This result suggests that complex **1** is a potential cytotoxic agent against cancer cells HeLa and MCF-7 for which the IC_{50} values are 18 and 16 μM, respectively. It is found that the anticancer activity of complex **1** is better than that of cisplatin. In particular, the results of *in vitro* cytotoxic activity indicate that the IC_{50} values of the synthesized complexes against non-cancerous human cell lines (NHDF and HEK) are found to be above 72 μM which indicates that complexes **1**–**4** are very specific towards cancer cell lines only. These results are displayed in Figure 9. Further *in vitro* investigations are underway in order to understand the mechanism of the antiproliferative activity of these complexes.

TABLE 6 Cytotoxicity of complexes **1**–**4** against various human cell lines

	IC_{50} (μM)[a]			
Compound	**HeLa**	**MCF-7**	**NHDF**	**HEK**
1	18 ± 0.6	16 ± 0.8	72 ± 0.8	>100
2	30 ± 1.1	38 ± 1.2	86 ± 1.0	>100
3	26 ± 0.8	32 ± 1.2	92 ± 0.6	>100
4	24 ± 0.8	28 ± 0.8	78 ± 0.8	>100
Cisplatin (standard)	22 ± 1.2	26 ± 1.2	76 ± 1.1	>100

[a]IC_{50} = concentration of drug required to inhibit growth of 50% of cancer cells (data are mean ± SD of three replicates each).

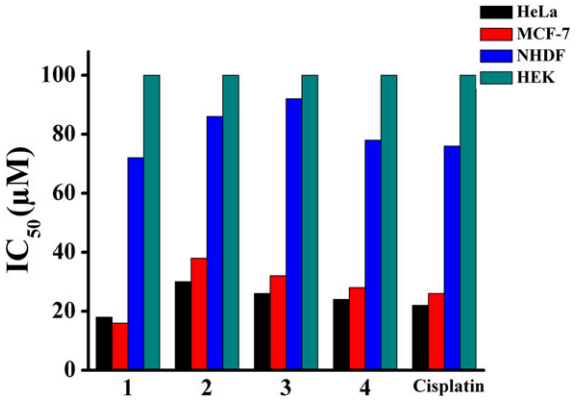

FIGURE 9 Trends in the inhibition of various human cell lines against synthesized complexes **1–4**

4 | CONCLUSIONS

The Knoevenagel condensate Schiff base (L) and its transition metal(II) complexes (**1–4**) have been synthesized and characterized using analytical and spectral methods. Based on the physicochemical analysis, these complexes adopt square planar geometry. The binding propensity of DNA towards the complexes has been studied using absorption spectrophotometric titration, cyclic voltammetry and viscosity measurements, which suggest that the complexes bind with CT DNA through the intercalation mode. The binding constant values disclose that the DNA binding affinity of the complexes lies in the order **1** > **4** > **3** > **2**. Fascinatingly, complex **1** exhibited potential antibacterial and antifungal activity against various microbial strains and proved to have better antimicrobial activity than the free ligand and other complexes. Gel electrophoresis experiment shows that the presence of hydrogen peroxide enhances the DNA cleavage to a significant extent. It has also been found that concentration plays a vital role in increasing the cleavage activity. Moreover, all the complexes show considerable cytotoxic activity against human cancer cell lines MCF-7 and HeLa but less toxicity against noncancerous human cell lines NHDF and HEK. In particular, complex **1** shows excellent cytotoxic activity against the two human tumour cell lines. All encouraging chemical and biological findings indicate that complex **1** is a suitable candidate for potential application as an anticancer drug. Further studies are needed to assess the *in vivo* pharmacological properties and to elucidate the actual mechanism of the biological activity.

ACKNOWLEDGEMENTS

The authors express their heartfelt thanks to the College Managing Board, Principal and Head of the Department of Chemistry, VHNSN College for providing necessary research facilities. IIT Bombay (SAIF) and IIT Chennai, India are gratefully acknowledged for providing instrumental facilities.

REFERENCES

[1] S. Kasibhatla, B. Tseng, *Mol. Cancer Ther.* **2003**, *2*, 573.

[2] P. Kahlem, B. Dörken, C. A. Schmitt, *J. Clin. Invest.* **2004**, *113*, 169.

[3] L. Kelland, *Nat. Rev. Cancer* **2007**, *7*, 573.

[4] M. J. Hannon, *Pure Appl. Chem.* **2007**, *79*, 2243.

[5] S. P. Fricker, *Dalton Trans.* **2007**, (43), 4903.

[6] E. R. Jamieson, S. J. Lippard, *Chem. Rev.* **1999**, *99*, 2467.

[7] P. Sathyadevi, P. Krishnamoorthy, R. R. Butorac, A. H. Cowley, N. S. P. Bhuvanesh, N. Dharmaraj, *Dalton Trans.* **2011**, *40*, 9690.

[8] A. G. Majouga, M. I. Zvereva, M. P. Rubtsova, D. A. Skvortsov, A. V. Mironov, D. M. Azhibek, O. O. Krasnovskaya, V. M. Gerasimov, A. V. Udina, N. I. Vorozhtsov, E. K. Beloglazkina, L. Agron, L. V. Mikhina, A. V. Tretyakova, N. V. Zyk, N. S. Zefirov, A. V. Kabanov, O. A. Dontsova, *J. Med. Chem.* **2014**, *57*, 6252.

[9] C. R. Kowol, R. Trondl, V. B. Arion, M. A. Jakupec, I. Lichtscheidl, B. K. Keppler, *Dalton Trans.* **2010**, *39*, 704.

[10] W. Al Zoubi, Y. Gun Ko, *J. Organometal. Chem.* **2016**, *822*, 173.

[11] B. Neto, A. Lapis, *Molecules* **2009**, *14*, 1725.

[12] P. R. Inamdar, R. Chauhan, J. Abraham, A. Sheela, *Inorg. Chem. Commun.* **2016**, *67*, 67.

[13] S. Chan, W. T. Wong, *Coord. Chem. Rev.* **1995**, *138*, 219.

[14] G. Prativel, J. Bernadou, B. Meunier, *Adv. Inorg. Chem.* **1998**, *45*, 251.

[15] Y. Xiong, L. N. Ji, *Coord. Chem. Rev.* **1996**, *185*, 711.

[16] V. Rajendiran, M. Murali, E. Suresh, K. Somasundaram, M. Palaniandavar, *Dalton Trans.* **2008**, (1), 148.

[17] S. Srinivasan, G. Rajagopal, P. R. Athappan, *Transition Met. Chem.* **2001**, *26*, 588.

[18] G. Menozzi, L. Mosti, L. Merello, A. Piana, U. Armani, M. Ghia, M. Angiola, F. Mattioli, *Il Farmaco* **2000**, *55*, 219.

[19] A. M. Asiri, S. A. Khan, *Molecules* **2010**, *15*, 6850.

[20] N. Raman, R. Jeyamurugan, R. Senthilkumar, B. Rajkapoor, S. G. Franzblau, *Eur. J. Med. Chem.* **2010**, *45*, 5438.

[21] S. Sumathi, P. Tharmaraj, C. D. Sheela, C. Anitha, *Spectrochim. Acta A* **2012**, *97*, 377.

[22] N. M. EI-Metwally, I. M. Gabr, A. M. Shallaby, *J. Coord. Chem.* **2005**, *58*, 1154.

[23] R. Prabhakaran, P. Kalaivani, R. Jayakumar, M. Zeller, A. D. Hunter, S. V. Renukadevi, E. Ramachandran, K. Natarajan, *Metallomics* **2011**, *3*, 42.

[24] K. Nakamoto, *Infrared and Raman Spectra of Inorganic and Coordination Compounds*, Wiley-Interscience, New York **1986**.

[25] A. B. P. Lever, *Inorganic Electronic Spectroscopy*, Elsevier, New York **1968**.

[26] A. A. Nejo, G. A. Kolawole, A. O. Nejo, *J. Coord. Chem.* **2010**, *63*, 4398.

[27] S. Srinivasan, G. Rajagopal, P. R. Athappan, *Transition Met. Chem.* **2001**, *26*, 588.

[28] B. J. Hathaway, A. A. G. Tomlinson, *Coord. Chem. Rev.* **1970**, *6*, 1.

[29] S. Belaid, A. Landreau, S. Djebbar, O. Benali-Baitich, G. Bouet, J. P. Bouchara, *J. Inorg. Biochem.* **2008**, *102*, 63.

[30] V. G. Vaidyanathan, B. U. Nair, *Eur. J. Inorg. Chem.* **2004**, *9*, 1840.

[31] F. Dimiza, A. N. Papadopoulos, V. Tangoulis, V. Psycharis, C. P. Raptopoulou, D. P. Kessissoglou, G. Psomas, *Dalton Trans.* **2010**, *39*, 4517.

[32] E. C. Long, J. K. Barton, *Acc. Chem. Res.* **1990**, *23*, 271.

[33] A. M. Pyle, J. P. Rehmann, R. Meshoyrer, C. V. Kumar, N. J. Turro, J. K. Barton, *J. Am. Chem. Soc.* **1989**, *111*, 3053.

[34] J. K. Barton, A. Danishefsky, J. M. Goldberg, *J. Am. Chem. Soc.* **1984**, *106*, 2172.

[35] F. Arjmand, F. Sayeed, D. Muddassir, *J. Photochem. Photobiol. B* **2011**, *103*, 166.

[36] P. R. Inamdar, A. Sheela, *J. Photochem. Photobiol. B* **2016**, *159*, 133.

[37] S. Tabassum, S. Parveen, F. Arjmand, *Acta Biomater.* **2005**, *1*, 677.

[38] L. Z. Li, C. Zhao, T. Xu, H. W. Ji, Y. H. Yu, G. Q. Guo, H. Chao, *J. Inorg. Biochem.* **2005**, *99*, 1076.

[39] P. Arthi, S. Shobana, P. Srinivasan, D. Prabhu, C. Arulvasu, A. Kalilur Rahiman, *J. Photochem. Photobiol. B* **2015**, *153*, 247.

[40] S. Satyanarayana, J. C. Dabrowiak, J. B. Chaires, *Biochemistry* **1992**, *31*, 9319.

[41] V. Thamilarasan, A. Jayamani, N. Sengottuvelan, *Eur. J. Med. Chem.* **2015**, *89*, 266.

[42] N. Raman, N. Pravin, *Eur. J. Med. Chem.* **2014**, *80*, 57.

[43] R. Paulpandiyan, N. Raman, *Appl. Organometal. Chem.* **2016**, *30*, 531.

[44] W. Al Zoubi, A. Ali Salih Al-Hamdani, M. Kaseem, *Appl. Organometal. Chem.* **2016**, *30*, 810.

[45] B. G. Tweedy, *Phytopathology* **1964**, *55*, 910.

[46] M. Kurtoğlu, M. M. Dağdelen, S. Toroğlu, *Transition Met. Chem.* **2006**, *31*, 382.

SUPPORTING INFORMATION

Additional Supporting Information may be found online in the supporting information tab for this article.

How to cite this article: Paulpandiyan R, Arunadevi A, Raman N. Role of Knoevenagel condensate pyrazolone derivative Schiff base ligated transition metal complexes in biological assay and cytotoxic efficacy. *Appl Organometal Chem*. 2017;e3792. https://doi.org/10.1002/aoc.3792